Title

Collision-Induced Dissociation Studies of Protonated Ions of Alkylated Thymidine and 2-Deoxyguanosine.

Journal

Journal of the American Society for Mass Spectrometry, 31(4)

Authors

Cui, Yuxiang
Yuan, Jun
Wang, Pengcheng
et al.

Publication Date

2020-04-01

DOI

10.1021/jasms.9b00147

Peer reviewed

HHS Public Access

Author manuscript

J Am Soc Mass Spectrom. Author manuscript; available in PMC 2021 April 01.

Published in final edited form as:

J Am Soc Mass Spectrom. 2020 April 01; 31(4): 927–937. doi:10.1021/jasms.9b00147.

Collision-Induced Dissociation Studies of Protonated Ions of Alkylated Thymidine and 2′-Deoxyguanosine

Yuxiang Cui, **Jun Yuan**, **Pengcheng Wang**

Environmental Toxicology Graduate Program, University of California Riverside, Riverside, California 92521, United States

Jun Wu,

Department of Chemistry, University of California Riverside, Riverside, California 92521, United States

Yang Yu,

Environmental Toxicology Graduate Program, University of California Riverside, Riverside, California 92521, United States

Yinsheng Wang

Environmental Toxicology Graduate Program and Department of Chemistry, University of California Riverside, Riverside, California 92521, United States

Abstract

Mass spectrometry and tandem MS (MS/MS) have been widely employed for the identification and quantification of damaged nucleosides in DNA, including those induced by alkylating agents. Upon collisional activation, protonated ions of alkylated nucleosides frequently undergo facile neutral loss of a 2-deoxyribose in MS/MS, and further cleavage of the resulting protonated nucleobases in MS^3 can sometimes be employed for differentiating regioisomeric alkylated DNA lesions. Herein, we investigated systematically the collision-induced dissociation (CID) of the protonated ions of O^4-alkylthymidine (O^4-alkyldT), O^2-alkyldT, O^6-alkyl-2′-deoxyguanosine (O^6-alkyldG), and N^2-alkyldG through MS^3 analysis. The MS^3 of O^2- and O^4-MedT exhibit different fragmentation patterns from each other and from other O^2- and O^4-alkyldT adducts carrying larger alkyl groups. Meanwhile, elimination of alkene via a six-membered ring transition state is the dominant fragmentation pathway for O^2-alkyldT, O^4-alkyldT, and O^6-alkyldG adducts carrying larger alkyl groups, whereas O^6-MedG mainly undergoes elimination of ammonia. The breakdown of N^2-alkyldG is substantially influenced by the structure of the alkyl group, where the relative ease in eliminating ammonia and alkene is modulated by the chain length and branching of the

Corresponding Author: Yinsheng Wang – Environmental Toxicology Graduate Program and Department of Chemistry, University of California Riverside, Riverside, California 92521, United States; Phone: (951)827-2700; yinsheng.wang@ucr.edu.
Complete contact information is available at: https://pubs.acs.org/10.1021/jasms.9b00147

Supporting Information

The Supporting Information is available free of charge at https://pubs.acs.org/doi/10.1021/jasms.9b00147.
MS/MS/MS of protonated ions of nucleosides, proposed fragmentation pathways, DFT-calculated fragmentation pathways and energy barriers, breakdown curves, and Cartesian coordinates for optimized structures of nucleobases and their breakdown products (PDF)

The authors declare no competing financial interest.

alkyl groups. We also rationalize our observations with density functional theory (DFT) calculations.

Graphical Abstract

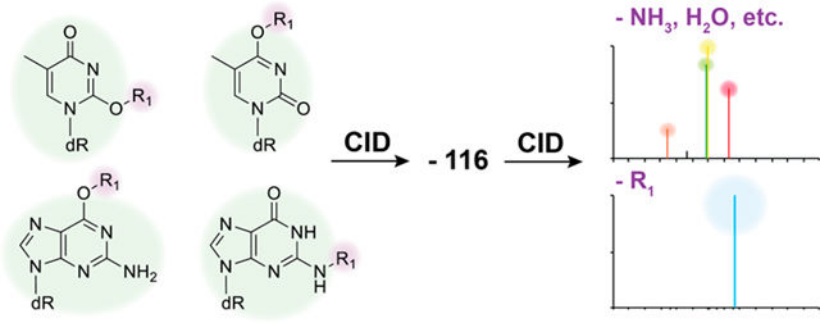

INTRODUCTION

Genome integrity is constantly challenged by exposure to endogenous metabolic byproducts and environmental toxicants, resulting in a wide array of DNA lesions, such as oxidative stress-induced DNA damage, alkylated DNA adducts, and heterocyclic aromatic amine (HAA)-induced DNA lesions.[1,2] Alkylation constitutes a major type of DNA damage, and alkylated DNA lesions can be produced from endogenous sources such as byproducts of lipid peroxidation or cellular methyl group donor (i.e., *S*-adenosyl-L-methionine) and from external sources such as tobacco smoke and chemotherapeutic drugs.[3,4]

Alkylation can occur at various heteroatoms in DNA, including oxygen and nitrogen atoms on nucleobases, as well as noncarbon-bonded oxygen atoms on backbone phosphate.[3,5,6] *N*7 and O^6 of guanine, *N*1 and *N*3 of adenine, and *N*3 of cytosine are the main alkylation sites on nucleobases, whereas N^6 and *N*7 of adenine, O^2, *N*3 and O^4 of thymine, O^2 of cytosine,[3,4,6] and N^2 of guanine can also be alkylated to a lesser extent.[6]

If not efficiently repaired, DNA alkylation adducts can lead to deleterious consequences including cell death or mutations. For example, alkylated DNA lesions can block replication and transcription, where the size of the alkyl group is positively correlated with their blockage effects.[7–13] In addition, O^6-alkyldG, O^4-alkyldT, and O^2-alkyldT are highly mutagenic:[5,6] O^6-alkyldG and O^4-alkyldT can readily mispair with thymine and guanine during DNA replication and result in G → A and T → C transitions, respectively.[4,7–9,11,14] Minor-groove O^2-alkylthymine is unfavorable in forming a base pair with any of the four canonical nucleobases in DNA, and elicits T → A and T → G transversions in *Escherichia coli* and HEK293T cells.[12,14,15] The minor-groove N^2-alkyldG adducts do not block replication or cause mutations in HEK293T cells, though depletion of certain translesion synthesis (TLS) polymerases can result in G → A and G → T mutations.[10]

Quantitative assessment about the formation and repair of DNA lesions is important for understanding their implications in human health. Liquid chromatography-tandem mass spectrometry (LC-MS/MS) coupled with the stable-isotope dilution method has become one

of the most widely used techniques for quantitative measurement of DNA lesions.[2,16] Aside from different retention behaviors on LC columns, some regioisomeric DNA adducts may be distinguished by their characteristic fragmentations in multistage MS. For instance, regioisomers of methylcytosine (e.g., *N*3-methylcytosine, N^4-methylcytosine and 5-methylcytosine),[17] methyluracil (5-methyluracil and *N*3-methyluracil)[18] and methyladenine (*N*1-methyladenine, 2-methyladenine, *N*3-methyladenine, N^6-methyladenine, and *N*7-methyladenine)[19] produce characteristic fragment ions that allow for the differentiation of regioisomers. On the other hand, the tandem mass spectra of *N*1- and N^2-methylguanine are indistinguishable from each other.[20] Investigation about the MS^n of regioisomeric alkylated DNA lesions may facilitate unambiguous identification of these DNA adducts.

Herein we investigated whether different regioisomers of alkylated thymidine and 2′-deoxyguanosine lesions can be distinguished by multistage MS in a linear ion-trap mass spectrometer. To this end, we acquired the collision-induced dissociation (CID) spectra of the protonated ions of a series of alkylated major-groove adducts O^4-alkylthymidine (O^4-alkyldT) and O^6-alkyl-2′-deoxyguanosine (O^6-alkyldG), and minor-groove adducts O^2-alkylthymidine (O^2-alkyldT) and N^2-alkyl-2′-deoxyguanosine (N^2-alkyldG) (Scheme 1). We also discuss the fragmentation pathways for these modified nucleosides and rationalize the observed cleavage pathways based on density functional theory (DFT) calculations.

EXPERIMENTAL METHODS

Materials.

All reagents, unless specifically noted, were purchased from Thermo Fisher Scientific. Synthetic standards of O^4-alkyldT and O^2-alkyldT were prepared following previously published procedures.[9,13] O^6-alkyldG- and N^2-alkyldG-containing oligodeoxyribonucleotides (ODNs) were previously synthesized.[8,12]

Nucleoside standards of O^6- and N^2-alkyldG were prepared from the enzymatic digestion of the corresponding lesion-containing ODNs following previously published procedures.[21] The resulting nucleoside mixtures were subsequently separated with a 4.6 × 250 mm Hypersil Gold C18 (Thermo Fisher Scientific, San Jose, CA) reversed-phase column, and the fractions containing the alkylation adducts were collected. The fractions were dried using a Speed-Vac and resuspended in doubly distilled water.

nLC-nESI-MS/MS/MS Experiments.

MS^3 experiments, which monitor the further cleavage of the $[M + H]^+$ ions of the nucleobase component of O^4-alkyldT, O^2-alkyldT, O^6-alkyldG, and N^2-alkyldG, were performed on an LTQ XL linear ion trap mass spectrometer equipped with a nanoelectrospray ionization source and coupled with an EASY-nLC II system (Thermo Fisher Scientific). In this vein, it is worth noting that the MS^3 experiments can also be conducted by direct fusion. We chose to employ nLC-nESI-MS/MS/MS because it is required for highly sensitive detection of DNA adducts in real samples (i.e., cellular and tissue DNA).

Synthetic alkylated nucleosides were first loaded onto a trapping column (150 μm × 40 mm) packed with porous graphitic carbon (PGC, 5 μm in particle size, Thermo Fisher Scientific) or Magic C18 AQ (5 μm in particle size, 200 Å in pore size, Michrom BioResources, Auburn, CA), at a flow rate of 2 μL/min within 7.5 min, followed by elution onto an analytical column (75 μm × 200 mm) packed with Zorbax SB-C18 stationary phase material (5 μm in particle size, 100 Å in pore size, Agilent Technologies, Santa Clara, CA) at a flow rate of 300 nL/min. Solutions A and B consisted of 0.1% (v/v) formic acid in water and acetonitrile, respectively. The nucleosides were eluted with a gradient of 0–16% B in 5 min, 16–22% B in 23 min, 22–50% B in 17 min, 50–90% B in 5 min, 90% B for 25 min, and the column was subsequently reequilibrated with 0% B.

Mass spectra were recorded in the positive-ion mode. The spray voltage was 2 kV and the capillary temperature was 275 °C. The capillary and tube lens voltages were 34 and 100 V, respectively. Automated gain control values were set at 3×10^4 and 1×10^3 for MS and MS^n, respectively. Normalized collisional energies, activation times, and isolation widths were set at 35% and 38%, 30 and 50 ms, and 3 and 2 *m*/*z* units for MS^2 and MS^3, respectively. The activation Q was 0.3 for both MS/MS and MS^3.

Breakdown Curves.

Breakdown curves for O^2- and O^4-alkyldT were constructed from ESI-MS/MS/MS acquired on an LTQ linear ion trap mass spectrometer (Thermo Fisher Scientific). These nucleosides were prepared in 5 μM aqueous solutions containing 50% methanol and 0.1% formic acid. The solutions were directly infused into the mass spectrometer at a flow rate of 3.0 μL/min with a syringe pump. The spray, capillary, and tube lens voltages were 5 kV, 1 and 95 V, respectively, and the temperature for the ion transfer tube was 300 °C. A normalized collisional energy of 35% was employed for MS^2, and those for MS^3 were in the range of 0–38%. The settings for automated gain control, precursor ion isolation, and ion activation were the same as those described above.

Breakdown curves for N^2- and O^6-alkyldG lesions were constructed from MS^3 acquired from online nLC-nESI-MS/MS/MS analysis following the above-described conditions, except that normalized collisional energies of 35% and 0–38% were employed for MS^2 and MS^3, respectively.

DFT Calculations.

DFT calculations at the B3LYP levels of theory with the 6–311+G(2d,2p) basis set were carried out using the Gaussian 09 package of program.[22] All optimized structures were subjected to vibrational frequency analysis for zero-point energy (ZPE) correction to the temperature of 298.15 K and the pressure of 1.0 atm. The vibrational frequency analysis was carried out to ensure that each transition state has only one imaginary vibrational frequency, whereas a local or global minimum displays no imaginary vibrational frequency. Transition state structures connecting their corresponding two adjacent minima were also confirmed by intrinsic reaction coordinate calculations. The energies discussed here represented the sum of electronic and thermal energies.

RESULTS AND DISCUSSION

The main objective of this study is to examine the fragmentation behaviors of protonated ions of regioisomeric alkylated dT and dG lesions in tandem MS. Since the $[M + H]^+$ ions of alkylated nucleosides undergo facile cleavage of the *N*-glycosidic bond in MS^2, producing the $[M + H]^+$ ions of the nucleobase portion,[23–25] we place our focus on the fragmentation of protonated nucleobases in MS^3.

Fragmentation of O^2-Alkylthymidine.

Collisional activation of the protonated O^2-methylthymine (*m*/*z* 141) gives rise to the fragment ions of *m*/*z* 123, 110, 109, and 84 (Figure 1a and Table S1), which we propose to arise from the neutral losses of H_2O, CH_3NH_2, CH_3OH, and CH_3NCO, respectively.

CID of protonated uracil, thymine, cytosine and some of their derivatives have been studied,[17,18,26–28] where the $[M + H]^+$ ions of unmodified pyrimidine bases undergo three major cleavage pathways, namely, neutral loss of NH_3, H_2O, or HNCO (Figure S1). Next we discuss the MS^3 spectra of O^2-MedT in the context of these three relevant pathways.

In the case of O^2-MedT, neutral loss of a CH_3NH_2 was observed in lieu of ammonia elimination (Figure 1a), suggesting the migration of the methyl group to a nitrogen atom prior to this neutral loss. In uracil, ammonia loss mainly originates from *N*3 (>90%), and only a small portion arises from *N*1 (<10%).[18,26,28] The O^2-methyl group may migrate to *N*3 or *N*1 due to their close proximity, which can subsequently lead to the loss of a CH_3NH_2.

Water elimination from protonated uracil can involve O^2 and O^4 at approximately equal frequency.[18,26] In the MS^3 of O^2-MedT, neutral losses of CH_3OH (*m*/*z* 109) and H_2O (*m*/*z* 123) are both observed (Figure 1a), with the former ion being more abundant than the latter. We propose that protonation of O^2, followed by the cleavage of C2–O2 bond, leads to the loss of CH_3OH.

Comparing with the CID of uracil, neutral loss of CH_3NCO (*m*/*z* 84) instead of HNCO is observed for O^2-MedT. Elimination of CH_3NCO can proceed through pathways analogous to the loss of HNCO from the $[M + H]^+$ ion of uracil, which was proposed to occur via a retro-Diels–Alder (RDA) mechanism (Scheme S1a),[18,28] though Beach and Gabryelski[26] suggested intramolecular nucleophilic attack as an alternative (Scheme S1b). C2 and O^2 are exclusively accountable for the carbon and oxygen losses in HNCO, respectively, with *N*3 contributing to the majority (90%) of the nitrogen loss.[18,26]

O^4 is the preferred protonation site in uracil,[18,26,29,30] and this preference is shifted toward O^2 with the presence of a 5-methyl group in thymidine.[31] Methylation at the O^2 position may also alter the preferential site of protonation in the nucleobase. We calculated the energies of several stable tautomers of protonated O^2-methylthymine (Scheme S2). Tautomer **3** with both O^2 and O^4 being in enol form and the O^2-methyl group and the O^4-hydrogen both pointing toward *N*3, which is analogous to the previously reported ground-state structures of protonated thymine and uracil,[32] displays the lowest energy. In a manner

similar to the case where the presence of an *N*3-methyl group in uracil can inhibit the formation of the enol tautomer,[33] the preferred protonation site for O^2-MedT is likely O^4, which can be considered as a result of stabilization by the O^2-methyl group. We assume that the conversions among these tautomers are achievable by proton transfer during ion activation process, as observed previously for some canonical nucleosides.[28,32,34] For example, tautomer **3** can be converted to tautomer **5** with a calculated energy barrier of 166.69 kJ/mol (Figure S2a).

The DFT-predicted energy barriers for the losses of CH_3OH, H_2O, and CH_3NH_2 from tautomer **5** are higher than that for the tautomerization (Figure 2a). The energy barriers for proton transfer in the pathways for the neutral losses of CH_3OH and H_2O are the same (243.63 kJ/mol), though the subsequent steps of CH_3OH elimination requires lower energy than that for the loss of H_2O. This is in line with the observation that the elimination of CH_3OH (*m*/*z* 109) is more facile than that of H_2O (*m*/*z* 123, Figure 2a). From another tautomer with the O^2-methyl group pointing toward *N*1 (tautomer **10** in Scheme S2), the energy barrier for the loss of CH_3NH_2 (247.26 kJ/mol, Figure S2c) is lower than that from tautomer **5** (256.72 kJ/mol, Figure 2a); therefore, CH_3NH_2 may also be eliminated from this tautomer. In addition, the calculated energy barrier for methyl group migration from O^2 to *N*3 (207.07 kJ/mol, Figure S2b) is lower than those for some of the pathways shown in Figure 2a and Figure S2b, suggesting the feasibility of the above-proposed mechanisms of methyl group migration prior to the elimination of CH_3NH_2 and CH_3NCO.

In contrast to O^2-MedT, fragmentation of Et-, *n*Pr-, *i*Pr- and *n*Bu-adducts all give rise to the predominant product ion of *m*/*z* 127 (Figure 1c,e; Figure S3a,c; and Table S1), which is assigned as the $[M + H]^+$ ion of thymine. The formation of this ion proceeds through the neutral loss of an alkene, probably via a six-membered ring transition state (Scheme 2).[35] Since the fragmentation of O^2-MedT cannot occur through this transition state, it undergoes fragmentation through pathways that are more similar to the unmodified dT. As a result, the energy barrier for the dissociation of O^2-EtdT is expected to be significantly lower than that of O^2-MedT. To test this hypothesis, we calculated the energy barrier for the dissociation of O^2-EtdT via a six-membered ring transition state (Figure 2b). The results indeed predict that this pathway requires a much lower activation energy (149.10 kJ/mol) than the dissociation pathways for O^2-MedT (Figure 2b).

Fragmentation of O^4-Alkylthymidine.

The major product ion in the MS^3 of protonated O^4-MedT arises from the neutral loss of a water from the modified nucleobase (*m*/*z* 123) (Figure 1b and Table S1). Fragment ions emanating from the eliminations of CH_3NCO (*m*/*z* 84) and CH_3OH (*m*/*z* 109) are also observed, with the relative abundances being approximately 10% and 4%, respectively. We again discuss the fragmentation pathway from the standpoint of the three major cleavage pathways for the protonated uracil.

In the case of O^4-MedT, loss of methylamine is no longer a major pathway, where the resulting fragment ion of *m*/*z* 110 is present at a very low abundance (<2% of total ions). For both O^2- and O^4-MedT, loss of NH_3 requires protonation of an NH group. However, owing

to the loss of an acidic proton upon alkylation, there is no third acidic proton available for the loss of the N as an NH_3.

Neutral loss of water predominates the MS^3 of O^4-MedT (~80% of total ions), while loss of CH_3OH occurs to a lesser extent. This elimination of water occurs much more readily for O^4-MedT than O^2-MedT, which might be attributed to the facile protonation of O^2 in O^4-MedT and the subsequent proton transfer from the neighboring *N*1 to O^2. We calculated the energies of different tautomers for protonated O^4-methylthymine, and the most stable one (tautomer **9**, Scheme S3) is indeed in enol form with both O^4-methyl group and 2-hydroxyl hydrogen atom pointing toward *N*3 (Scheme S3). The DFT-calculated energy barrier for the above-mentioned pathway for this tautomer is 244.95 kJ/mol (Figure 2c), which is not much different from that for O^2-MedT (Figure 2a, 243.63 kJ/mol for loss of CH_3OH). On the other hand, elimination of CH_3OH, which is more facile from a different tautomer, requires tautomerization (Figure S4) and exhibits a higher energy barrier (278.04 kJ/mol, Figure 2c), thereby rendering it less likely to occur.

Similar to what we found for O^2-MedT, we observed the elimination of CH_3NCO in the MS^3 of O^4-MedT. This loss may again proceed through methyl group migration (i.e., from O^4 to *N*3) followed by ring cleavage. In this vein, methyl group was previously shown to migrate from quaternary ammonium moieties during collisional activation of peptides and a metabolite.[36,37] Other potential pathways for CH_3NCO elimination are shown in Scheme S1c–e, and further experiments are needed for the elucidation of the cleavage mechanisms for this neutral loss.

Unlike the aforementioned methylated dT adducts, Et-, *n*Pr-, *i*Pr- and *n*Bu-dT adducts are very similar among the O^2 and O^4 regioisomers, where protonated thymine dominates the MS^3 (*m*/*z* 127) (Figure 1d,f; Figure S3b,d; and Table S1). We again propose that the elimination of alkene proceeds via a six-membered ring transition state (Scheme 2b). We calculated the energy barrier for the loss of ethylene from O^4-EtdT (164.03 kJ/mol), and it is indeed much lower than that of H_2O or CH_3OH elimination from O^4-MedT (Figure 2c,d). The differences in fragmentation behaviors for the *O*-methylated and other *O*-alkylated thymidine lesions in MS^3 prompted us to examine the differences in collisional energy required for the fragmentation of these modified nucleobases. To this end, we acquired the breakdown curves for the aforementioned O^2- and O^4-alkyldT adducts by varying the collisional energy employed in the MS^3 fragmentation step and plotting the percentage of precursor ion among all the ions found in MS^3 (Figure 3). In this vein, we kept the collisional energy for MS^2 consistent while acquiring the MS^3. Our results showed that breakdown curves for the protonated ions of the nucleobase portions of O^2-MedT and O^4-MedT are nearly identical, but differ markedly from those of other O^2- and O^4-alkyldT lesions (Figure 3).

The similarity in the break down curves for O^2-MedT and O^4-MedT is in accordance with the similar calculated energy barriers for the fragmentation of O^2-MedT and O^4-MedT. When compared with the methyl adducts, the corresponding Et-, *n*Pr-, *i*Pr- and *n*Bu-adducts require much lower energy to fragment (Figure 3), which is also reflected by DFT calculation results for the methyl and ethyl adducts (Figure 2). The nearly identical

breakdown curves for the O^2-alkyldT lesions and the O^4-alkylated counterparts suggest that the collisional energies required for the fragmentation of the protonated ions of their nucleobase portions do not allow for the differentiation of these regioisomeric pairs of *O*-alkylated dT lesions.

The differences in fragmentation pathways of O^2-MedT and O^4-MedT are likely also attributable partly to the tautomers in the ion ensembles in the linear ion trap. Along this line, it has been demonstrated, both theoretically and experimentally, that different tautomers of nucleobases can exist simultaneously.[30–32,38–40] For O^2-MedT, the most stable tautomer (Scheme S2 tautomer **3**) is conducive for the loss of CH_3OH; the elimination of H_2O, however, can occur directly from the less stable, hence the less abundant, tautomer **2** or **7** (Scheme S2). In the case of O^4-MedT, the most stable tautomer (tautomer **9**, Scheme S3) is in a conformation that is highly favorable for the loss of H_2O via proton transfer, as noted above.

Fragmentation of O^6-Alkyl-2′-deoxyguanosine.

The O^6-alkyldG lesions behave similarly to the O^2-alkyldT and O^4-alkyldT adducts in the respect that the MS^3 of O^6-MedG differs significantly from those of other O^6-alkyldG adducts. In particular, the protonated nucleobase of O^6-MedG mainly undergoes neutral loss of an ammonia, whereas those of other O^6-alkyldG adducts lose readily the corresponding neutral alkenes (Figure 4 and Table S2).

Collision-induced dissociation of protonated guanine mainly undergoes two fragmentation pathways, namely losses of an ammonia and a cyanamide (NH_2CN) or carbodiimide (HN=C=NH).[20,41] During CID of the $[M + H]^+$ ion of guanine, $N1$ and N^2 nitrogen atoms lose their identities after ring-opening at the $N1$−C6 bond.[20] In the case of O^6-MedG, the main fragment ion results from the elimination of an ammonia. We also observed, in low abundance, the ion of m/z 110, which likely originates from the loss of a CH_3N=C=NH. We compared the energies for different tautomers of protonated O^6-methylguanine (Scheme S4) at a lower level of theory and chose the most stable tautomer for computation at higher levels of theory. DFT calculation results for the most stable tautomer (tautomer **11** in Scheme S4) indicate that the energy barrier for proton transfer from $N3$ to N^2 is 195.72 kJ/mol (Figure 5a), and the ensuing product can readily eliminate an NH_3 with a calculated activation energy of 228.94 kJ/mol (Figure 5a). The ion of m/z 167 may be attributed to the loss of an ammonia from a water molecule adduct, as described previously.[42]

MS^3 of the bulkier O^6-alkyldG lesions, including Et-, *n*Pr-, *i*Pr-, *n*Bu-, *i*Bu-, *s*Bu-adducts, all show the predominant fragment ion of protonated guanine (m/z 152). This again can be attributed to the facile loss of the corresponding alkene via a six-membered ring transition state (Scheme 2c). The loss of an alkene is more facile than that of ammonia via the ring-opening pathway in the CID of guanine. The DFT-calculated energy barrier for the loss of ethylene from O^6-EtdG is 162.68 kJ/mol, and those for the loss of propene from O^6-*n*PrdG and O^6-*i*PrdG are 157.98 and 128.96 kJ/mol, respectively (Figure 5b and Figure S5), which are substantially lower than that for proton transfer within protonated O^6-MedG (195.72 kJ/mol) and the subsequent elimination of ammonia (228.94 kJ/mol) (Figure 5a). This is in keeping with the facile loss of alkene observed in MS^3.

Fragmentation of N^2-Alkyl-2′-deoxyguanosine.

The fragmentations of N^2-alkyldG adducts exhibit similarities and differences when compared with their O^6 counterparts, where collisional activation of the protonated nucleobases of N^2-MedG, N^2-EtdT, N^2-*n*PrdG and N^2-*n*BudG leads to the facile loss of an ammonia in MS^3; CID of the $[M + H]^+$ ions of the nucleobases of N^2-*i*PrdG, N^2-*i*BudG and N^2-*s*BudG, however, produce protonated guanine as the dominant product ion in MS^3 (Figure 6 and Table S2).

The MS^3 of N^2-MedG is very similar to that of O^6-MedG, except for the slight differences in relative abundances of fragment ions, making it difficult to distinguish the two regioisomers using MS^3. Along this line, the predominant loss of ammonia (*m*/*z* 149) from protonated N^2-methylguanine is consistent with previously published CID spectrum acquired for the FAB-produced $[M + H]^+$ ion.[20]

For those lesions carrying a straight-chain alkyl group, we observed a progressive elevation in the abundance of fragment ion from the loss of an alkene and a concomitant decrease in that from the elimination of an ammonia as the chain length increases. The most abundant fragment ion found for the MS^3 of N^2-EtdG forms from the elimination of ammonia. Unlike the MS^3 of the aforementioned *O*-ethylated adducts, where the product ion emanating from the loss of ethylene dominates the spectrum, the fragment ion from the loss of ethylene (*m*/*z* 152) is present, albeit not as abundant as that arising from the loss of NH_3 (*m*/*z* 163), in the MS^3 of N^2-EtdG. We observed that the abundance of the *m*/*z*-152 ion increases further in the MS^3 of N^2-*n*PrdG (Figure 6c) and it surpasses the ion from the neutral loss of ammonia (*m*/*z* 191) in the MS^3 of N^2-*n*BudG (Figure 6d). The MS^3 of N^2-*i*BudG showed a further increase in the abundance of the *m*/*z*-152 ion and decrease in the *m*/*z*-191 ion (Figure 6f). Elimination of ammonia is not detectable in the MS^3 of N^2-*i*PrdG and N^2-*s*BudG (Figure 6e,g), suggesting that the branched alkyl chain facilitates the loss of alkene while concomitantly suppressing the neutral loss of ammonia.

We next assessed the energy barriers for the fragmentation of the two N^2-PrdG adducts. DFT-calculated energy barriers for the elimination of ammonia from N^2-*n*PrdG and N^2-*i*PrdG do not differ significantly (i.e., 241.90 and 241.10 kJ/mol, respectively, Figure 7a,c). DFT-calculated energy barriers for tautomerization from the most stable tautomers to the precursor for ammonia elimination are shown in Figure S6, where the pathway for ammonia loss from these tautomers is likely dependent on hydrogen transfer. The elimination of an alkene via the six-membered ring transition state for N^2-*i*PrdG (Figure 7d) exhibits a much lower energy barrier than that for N^2-*n*PrdG (Figure 7b), which are 209.37 and 235.93 kJ/mol, respectively. We reason that alkylation of N^2 may impede the formation of the six-membered ring transition state relative to their O^6-alkyldG counterparts; hence, the ease in the formation of a six-membered ring transition state determines the fragmentation pathway for N^2-alkyldG adducts.

The ions of *m*/*z* 167, 181, 195, and 209 found in MS^3 of N^2-MedG, N^2-EtdG, N^2-*n*PrdG, and N^2-*n*BudG can be attributed to ion-neutral reactions between the precursor ions and residual H_2O molecule, followed by the loss of an ammonia.[42–45] The instrument conditions for MS^3 acquisition are identical for O^6-alkyldG and N^2-alkyldG, yet we observed more

water molecule adducts in the spectra of N^2-alkyldG; the exact reason for this difference is unclear.

The above results showed that, while some of the N^2- and O^6-alkyldG lesions (i.e., when alkyl group = Et, *n*Pr, *n*Bu and *i*Bu) can be distinguished on the basis of their MS^3, others (i.e., when alkyl group = Me, *i*Pr, and *s*Bu) are nearly identical. Our DFT calculation results also showed that the energy barriers for the elimination of alkenes from the protonated nucleobases of O^6-*n*PrdG and O^6-*i*PrdG are much lower than the corresponding alkene losses from the regioisomeric N^2-*n*PrdG and N^2-*i*PrdG (Figure S5 and Figure 7). Hence, we also explored whether the latter groups of lesions could be differentiated on the basis of differences in collisional energies required for fragmenting the protonated ions of their nucleobases. To this end, we acquired the breakdown curves for the fragmentations of the protonated nucleobases of the regioisomeric pairs of N^2- and O^6-alkyldG lesions with the alkyl group being a Me, *i*Pr, *i*Bu, and *s*Bu. N^2- and O^6-*i*BudG were included because the characteristic *m*/*z*-191 peak resulting from ammonia elimination exists at a relatively low abundance, which may not be observable when the collisional energy is not high enough. It turned out that the collisional energies required for the fragmentations of N^2-alkylated lesions are higher than those for the O^6-alkylated counterparts when the alkyl group is *i*Pr, *i*Bu, or *s*Bu (Figure 8). The breakdown curves for N^2- and O^6-MedG are, however, almost identical (Figure S7). Together, the above results demonstrate that collision energies required for fragmentation can facilitate the differentiation of those regioisomeric pairs of alkyldG lesions with a branched chain alkyl group.

CONCLUSIONS

We acquired the MS^3 for the protonated ions of a series of O^2- and O^4-alkyldT as well as O^6- and N^2-alkyldG adducts. We observed interesting fragmentation behaviors for those alkylated DNA lesions that are dependent on the chain lengths of the alkyl groups. In particular, exocyclic *O*-methylated adducts (O^2-MedT, O^4-MedT, and O^6-MedG) exhibit unique fragmentation pathways compared with adducts bearing larger alkyl groups at the same positions on nucleobases. Elimination of methylamine and methanol were the predominant fragmentation pathways for the protonated nucleobase of O^2-MedT, whereas the neutral losses of water and ammonia are the dominant pathway for O^4-MedT and O^6-MedG, respectively. O^2- and O^4-alkyldT, and O^6-alkyldG (alkyl = -Et, -*n*Pr, -*i*Pr, -*n*Bu and, for O^6-alkyldG, -*i*Bu, and -*s*Bu) with larger alkyl groups undergo facile loss of alkene from a six-membered ring transition state. Our DFT calculation results show that the energy barrier for the elimination of ethylene from ethyl adducts is easily attainable during the CID processes, which is consistent with the results from the breakdown curves and is in support of the involvement of a six-membered ring transition state.

N^2-alkyldG adducts behave differently from the above-mentioned *O*-alkylated adducts in CID, where neutral loss of ammonia was the predominant pathway for N^2-MedG, which is indistinguishable from that for O^6-MedG. The fragmentation pathways for N^2-alkyldG lesions with larger alkyl groups are dependent on the bulkiness of the alkyl chain, which is attributed to the relative ease in the formation of the six-membered ring transition state.

The results from our study also showed that, except for the methyl adducts, the MS^3 of O^2- and O^4-alkyldT are indistinguishable. Except for the methyl adducts, the regioisomeric O^6- and N^2-alkyldG can be differentiated on the basis of the relative ease in NH_3 loss, or on the basis of differences in collisional energy required for the fragmentation. For the adducts that cannot be distinguished based on MS^n, such as regioisomeric O^2- and O^4-alkyldT, as well as O^6- and N^2-MedG, separation techniques (i.e., liquid chromatography[46] and ion mobility[47,48]) are required for their differentiation.

Together, our tandem mass spectrometric and computational studies provide new insights into the fragmentations of protonated ions of alkylated thymidine and 2′-deoxyguanosine derivatives. This study may be useful to those who are interested in characterizing DNA adducts using multistage mass spectrometry and those who study the fragmentation mechanisms in CID. We hope that the results presented in this study will be useful to those researchers who are interested in elucidating the CID mechanisms by computational calculations, ion mobility mass spectrometry, and other techniques. Studies with these approaches may further elucidate the mechanisms involved in the fragmentation of alkylated nucleosides and nucleobases. In addition, selective stable isotope labeling of these alkylated DNA lesions may allow for revealing the origins of the nitrogen atom(s) involved in the loss of NH_3 from protonated nucleobases of O^6-MedG and N^2-alkyldG, and for substantiating the notion about the involvement of methyl group migration in the fragmentation of the protonated nucleobase portions of O^4- and O^2-MedT.

Supplementary Material

Refer to Web version on PubMed Central for supplementary material.

ACKNOWLEDGMENTS

The authors would like to thank the National Institutes of Health for Supporting this research (R01 ES029749), and Dr. Xiaomei He for providing the N^2-*n*BudG-containing ODN.

REFERENCES

(1). Sancar A; Lindsey-Boltz LA;Ünsal-Kacmaz K; Linn S Molecular mechanisms of mammalian DNA repair and the DNA damage checkpoints. Annu. Rev. Biochem 2004, 73, 39–85. [PubMed: 15189136]

(2). Yu Y; Wang P; Cui Y; Wang Y Chemical analysis of DNA damage. Anal. Chem 2018, 90, 556–576. [PubMed: 29084424]

(3). Fu D; Calvo JA; Samson LD Balancing repair and tolerance of DNA damage caused by alkylating agents. Nat. Rev. Cancer 2012, 12, 104–120. [PubMed: 22237395]

(4). Shrivastav N; Li DY; Essigmann JM Chemical biology of mutagenesis and DNA repair: cellular responses to DNA alkylation. Carcinogenesis 2010, 31, 59–70. [PubMed: 19875697]

(5). Drablos F; Feyzi E; Aas PA; Vaagbo CB; Kavli B; Bratlie MS; Pena-Diaz J; Otterlei M; Slupphaug G; Krokan HE Alkylation damage in DNA and RNA - repair mechanisms and medical significance. DNA Repair 2004, 3, 1389–1407. [PubMed: 15380096]

(6). Puyo S; Montaudon D; Pourquier P From old alkylating agents to new minor groove binders. Crit. Rev. Oncol. Hemat 2014, 89, 43–61.

(7). Du H; Wang PC; Li L; Wang YS Repair and translesion synthesis of O^6-alkylguanine DNA lesions in human cells. J. Biol. Chem 2019, 294, 11144–11153. [PubMed: 31167778]

(8). Wang P; Wang Y Cytotoxic and mutagenic properties of O6-alkyl-2′-deoxyguanosine lesions in *Escherichia coli* cells. J. Biol. Chem 2018, 293, 15033–15042. [PubMed: 30068548]

(9). Wang PC; Amato NJ; Zhai QQ; Wang YS Cytotoxic and mutagenic properties of O^4-alkylthymidine lesions in *Escherichia coli* cells. Nucleic Acids Res. 2015, 43, 10795. [PubMed: 26400162]

(10). Wu J; Du H; Li L; Price NE; Liu XC; Wang YS The impact of minor-groove N^2-alkyl-2′-deoxyguanosine lesions on DNA replication in human cells. ACS Chem. Biol 2019, 14, 1708–1716. [PubMed: 31347832]

(11). Wu J; Li L; Wang PC; You CJ; Williams NL; Wang YS Translesion synthesis of O^4-alkylthymidine lesions in human cells. Nucleic Acids Res. 2016, 44, 9256–9265. [PubMed: 27466394]

(12). Wu J; Wang PC; Li L; You CJ; Wang YS Cytotoxic and mutagenic properties of minor-groove O^2-alkylthymidine lesions in human cells. J. Biol. Chem 2018, 293, 8638–8644. [PubMed: 29685891]

(13). Zhai QQ; Wang PC; Cai Q; Wang YS Syntheses and characterizations of the *in vivo* replicative bypass and mutagenic properties of the minor-groove O^2-alkylthymidine lesions. Nucleic Acids Res. 2014, 42, 10529–10537. [PubMed: 25120272]

(14). Zhai QQ; Wang PC; Wang YS Cytotoxic and mutagenic properties of regioisomeric O^2-, N3-and O^4-ethylthymidines in bacterial cells. Carcinogenesis 2014, 35, 2002–2006. [PubMed: 24710626]

(15). Andersen N; Wang JS; Wang PC; Jiang Y; Wang YS *In vitro* replication studies on O^2-methylthymidine and O^4-methylthymidine. Chem. Res. Toxicol 2012, 25, 2523–2531. [PubMed: 23113558]

(16). Tretyakova N; Goggin M; Sangaraju D; Janis G Quantitation of DNA adducts by stable isotope dilution mass spectrometry. Chem. Res. Toxicol 2012, 25, 2007–2035. [PubMed: 22827593]

(17). Jensen SS; Ariza X; Nielsen P; Vilarrasa J; Kirpekar F Collision-induced dissociation of cytidine and its derivatives. J. Mass Spectrom 2007, 42, 49–57. [PubMed: 17149798]

(18). Nelson CC; McCloskey JA Collision-induced dissociation of uracil and its derivatives. J. Am. Soc. Mass Spectrom 1994, 5, 339–349. [PubMed: 24222588]

(19). Nelson CC; McCloskey JA Collision-induced dissociation of adenine. J. Am. Chem. Soc 1992, 114, 3661–3668.

(20). Gregson JM; McCloskey JA Collision-induced dissociation of protonated guanine. Int. J. Mass Spectrom. Ion Processes 1997, 165, 475–485.

(21). Wang J; Yuan BF; Guerrero C; Bahde R; Gupta S; Wang YS Quantification of oxidative DNA lesions in tissues of Long-Evans Cinnamon rats by capillary high-performance liquid chromatography-tandem Mass spectrometry coupled with stable isotope-dilution method. Anal. Chem 2011, 83, 2201–2209. [PubMed: 21323344]

(22). Frisch MJ; Trucks GW; Schlegel HB; Scuseria GE; Robb MA; Cheeseman JR; Scalmani G; Barone V; Mennucci B; Petersson GA; Nakatsuji H; Caricato M; Li X; Hratchian HP; Izmaylov AF; Bloino J; Zheng G; Sonnenberg JL; Hada M; Ehara M; Toyota K; Fukuda R; Hasegawa J; Ishida M; Nakajima T; Honda Y; Kitao O; Nakai H; Vreven T; Montgomery JA Jr.; Peralta JE; Ogliaro F; Bearpark M; Heyd JJ; Brothers E; Kudin KN; Staroverov VN; Kobayashi R; Normand J; Raghavachari K; Rendell A; Burant JC; Iyengar SS; Tomasi J; Cossi M; Rega N; Millam JM; Klene M; Knox JE; Cross JB; Bakken V; Adamo C; Jaramillo J; Gomperts R; Stratmann RE; Yazyev O; Austin AJ; Cammi R; Pomelli C; Ochterski JW; Martin RL; Morokuma K; Zakrzewski VG; Voth GA; Salvador P; Dannenberg JJ; Dapprich S; Daniels AD; Farkas O; Foresman JB; Ortiz JV; Cioslowski J; Fox DJ Gaussian 09 Rev. A.02; Gaussian, Inc.: Wallingford, CT, 2009.

(23). Balbo S; Turesky RJ; Villalta PW DNA adductomics. Chem. Res. Toxicol 2014, 27, 356–366. [PubMed: 24437709]

(24). Fryčák P; Hušková R; Adam T; Lemr K Atmospheric pressure ionization mass spectrometry of purine and pyrimidine markers of inherited metabolic disorders. J. Mass Spectrom 2002, 37, 1242–1248. [PubMed: 12489084]

(25). Tretyakova N; Villalta PW; Kotapati S Mass spectrometry of structurally modified DNA. Chem. Rev 2013, 113, 2395–2436. [PubMed: 23441727]

(26). Beach DG; Gabryelski W Revisiting the reactivity of uracil during collision induced dissociation: tautomerism and charge-directed processes. J. Am. Soc. Mass Spectrom 2012, 23, 858–868. [PubMed: 22351291]

(27). Cao H; Wang Y Collisionally activated dissociation of protonated 2′-deoxycytidine, 2′-deoxyuridine, and their oxidatively damaged derivatives. J. Am. Soc. Mass Spectrom 2006, 17, 1335–1341. [PubMed: 16872831]

(28). Molina ER; Ortiz D; Salpin J-Y; Spezia R Elucidating collision induced dissociation products and reaction mechanisms of protonated uracil by coupling chemical dynamics simulations with tandem mass spectrometry experiments. J. Mass Spectrom 2015, 50, 1340–1351. [PubMed: 26634967]

(29). Tuytten R; Lemière F; Esmans EL; Herrebout WA; van der Veken BJ; Dudley E; Newton RP; Witters E In-source CID of guanosine: gas phase ion–molecule reactions. J. Am. Soc. Mass Spectrom 2006, 17, 1050–1062. [PubMed: 16750381]

(30). Wu RR; Yang B; Frieler CE; Berden G; Oomens J; Rodgers MT Diverse mixtures of 2,4-dihydroxy tautomers and O4 protonated conformers of uridine and 2′-deoxyuridine coexist in the gas phase. Phys. Chem. Chem. Phys 2015, 17, 25978–25988. [PubMed: 26225730]

(31). Wu RR; Yang B; Frieler CE; Berden G; Oomens J; Rodgers MT 2,4-Dihydroxy and O2 protonated tautomers of dThd and Thd coexist in the gas phase: methylation alters protonation preferences versus dUrd and Urd. J. Am. Soc. Mass Spectrom 2016, 27, 410–421. [PubMed: 26676730]

(32). Salpin J-Y; Guillaumont S; Tortajada J; MacAleese L; Lemaire J; Maitre P Infrared spectra of protonated uracil, thymine and cytosine. ChemPhysChem 2007, 8, 2235–2244. [PubMed: 17910021]

(33). Salpin J-Y; Haldys V; Steinmetz V; Léon E; Yáñez M; Montero-Campillo MM Protonation of methyluracils in the gas phase: the particular case of 3-methyluracil. Int. J. Mass Spectrom 2018, 429, 47–55.

(34). Wu R; McMahon TB Investigation of proton transport tautomerism in clusters of protonated nucleic acid bases (cytosine, uracil, thymine, and adenine) and ammonia by high-pressure mass spectrometry and ab initio calculations. J. Am. Chem. Soc 2007, 129, 569–580. [PubMed: 17227020]

(35). Boer FP; Shannon TW; McLafferty FW Electronic structure of the six-membered cyclic transition state in some.gamma.-hydrogen rearrangements. J. Am. Chem. Soc 1968, 90, 7239–7248.

(36). Griffith CM; Williams PB; Tinoco LW; Dinges MM; Wang Y; Larive CK ^{1}H NMR metabolic profiling of earthworm (*Eisenia fetida*) coelomic fluid, coelomocytes, and tissue: identification of a new metabolite–malylglutamate. J. Proteome Res 2017, 16, 3407–3418. [PubMed: 28753027]

(37). Xiong L; Ping L; Yuan B; Wang Y Methyl group migration during the fragmentation of singly charged ions of trimethyllysine-containing peptides: precaution of using MS/MS of singly charged ions for interrogating peptide methylation. J. Am. Soc. Mass Spectrom 2009, 20, 1172–1181. [PubMed: 19303795]

(38). Anwar A; Psutka J; Walker SWC; Dieckmann T; Janizewski JS; Larry Campbell J; Scott Hopkins W Separating and probing tautomers of protonated nucleobases using differential mobility spectrometry. Int. J. Mass Spectrom 2018, 429, 174–181.

(39). Colominas C; Luque FJ; Orozco M Tautomerism and protonation of guanine and cytosine. Implications in the formation of hydrogen-bonded complexes. J. Am. Chem. Soc 1996, 118, 6811–6821.

(40). Podolyan Y; Gorb L; Leszczynski J Protonation of nucleic acid bases. A comprehensive post-Hartree–Fock study of the energetics and proton affinities. J. Phys. Chem. A 2000, 104, 7346–7352.

(41). Qian M; Yang S; Wu H; Majumdar P; Leigh N; Glaser R Ammonia elimination from protonated nucleobases and related synthetic substrates. J. Am. Soc. Mass Spectrom 2007, 18, 2040–2057. [PubMed: 17920289]

(42). Tuytten R; Lemièere F; Van Dongen W; Esmans EL; Witters E; Herrebout W; Van Der Veken B; Dudley E; Newton RP Intriguing mass spectrometric behavior of guanosine under low energy collision-induced dissociation: H_2O adduct formation and gas-phase reactions in the collision cell. J. Am. Soc. Mass Spectrom 2005, 16, 1291–1304. [PubMed: 15979336]

(43). Alechaga É; Moyano E; Galceran MT Ion–molecule adduct formation in tandem mass spectrometry. Anal. Bioanal. Chem 2016, 408, 1269–1277. [PubMed: 26700446]

(44). Beach DG; Gabryelski W Solution to collision induced dissociation mass spectrometry challenge. Anal. Bioanal. Chem 2018, 410, 3927–3930. [PubMed: 29926153]

(45). Sultan J Collision induced dissociation of deprotonated guanine: fragmentation of pyrimidine ring and water adduct formation. Int. J. Mass Spectrom 2008, 273, 58–68.

(46). Cui Y; Wang P; Yu Y; Yuan J; Wang Y Normalized retention time for targeted analysis of the DNA adductome. Anal. Chem 2018, 90, 14111–14115. [PubMed: 30500177]

(47). Quinn R; Basanta-Sanchez M; Rose RE; Fabris D Direct infusion analysis of nucleotide mixtures of very similar or identical elemental composition. J. Mass Spectrom 2013, 48, 703–712. [PubMed: 23722961]

(48). Rose RE; Quinn R; Sayre JL; Fabris D Profiling ribonucleotide modifications at full-transcriptome level: a step toward MS-based epitranscriptomics. RNA 2015, 21, 1361–1374. [PubMed: 25995446]

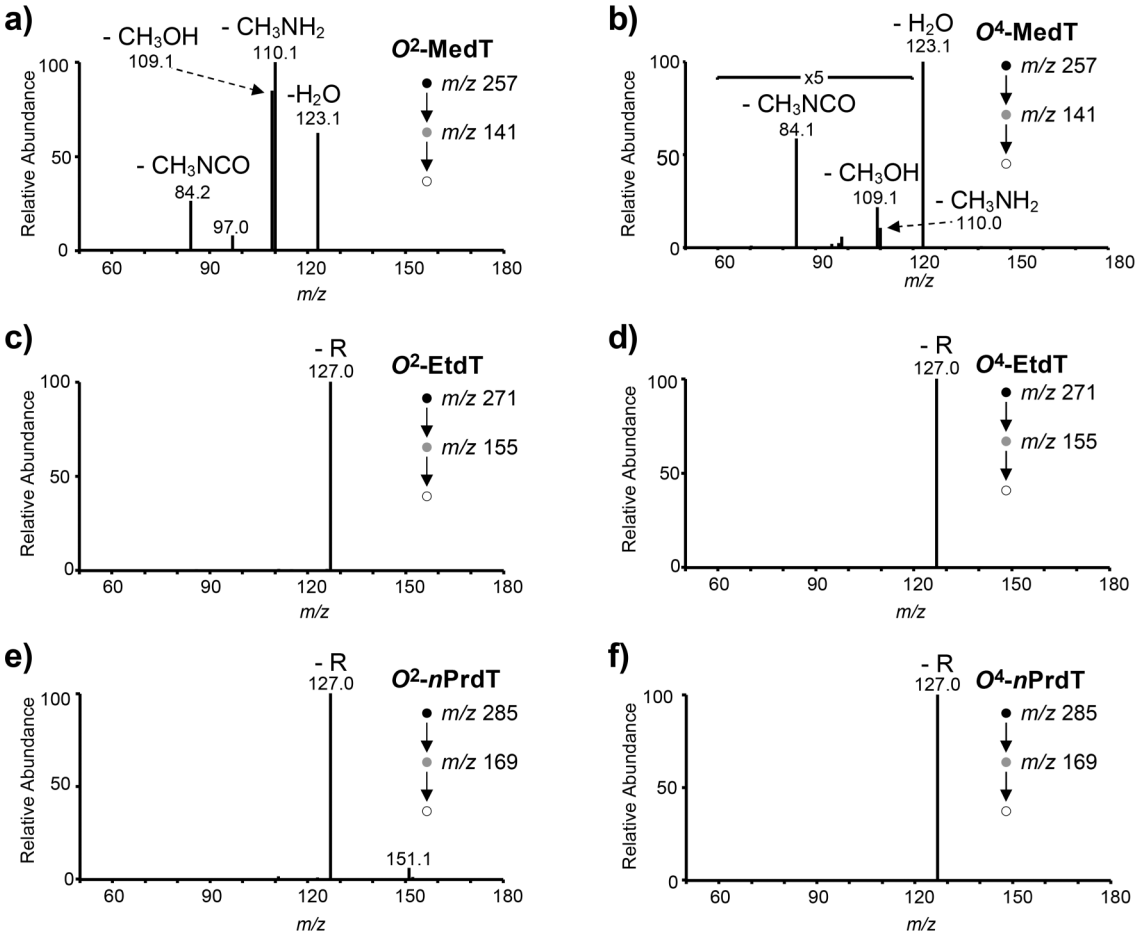

Figure 1.

MS^3 of: (a) O^2-MedT, (b) O^4-MedT, (c) O^2-EtdT, (d) O^4-EtdT, (e) O^2-*n*PrdT, and (f) O^4-*n*PrdT acquired from nLC-nESI-MS/MS/MS experiments. The line labeled with "×5" in (b) indicates the *m*/*z* range of the spectrum (*m*/*z* 60–120) that was amplified by 5 times to better visualize the fragment ions in the region.

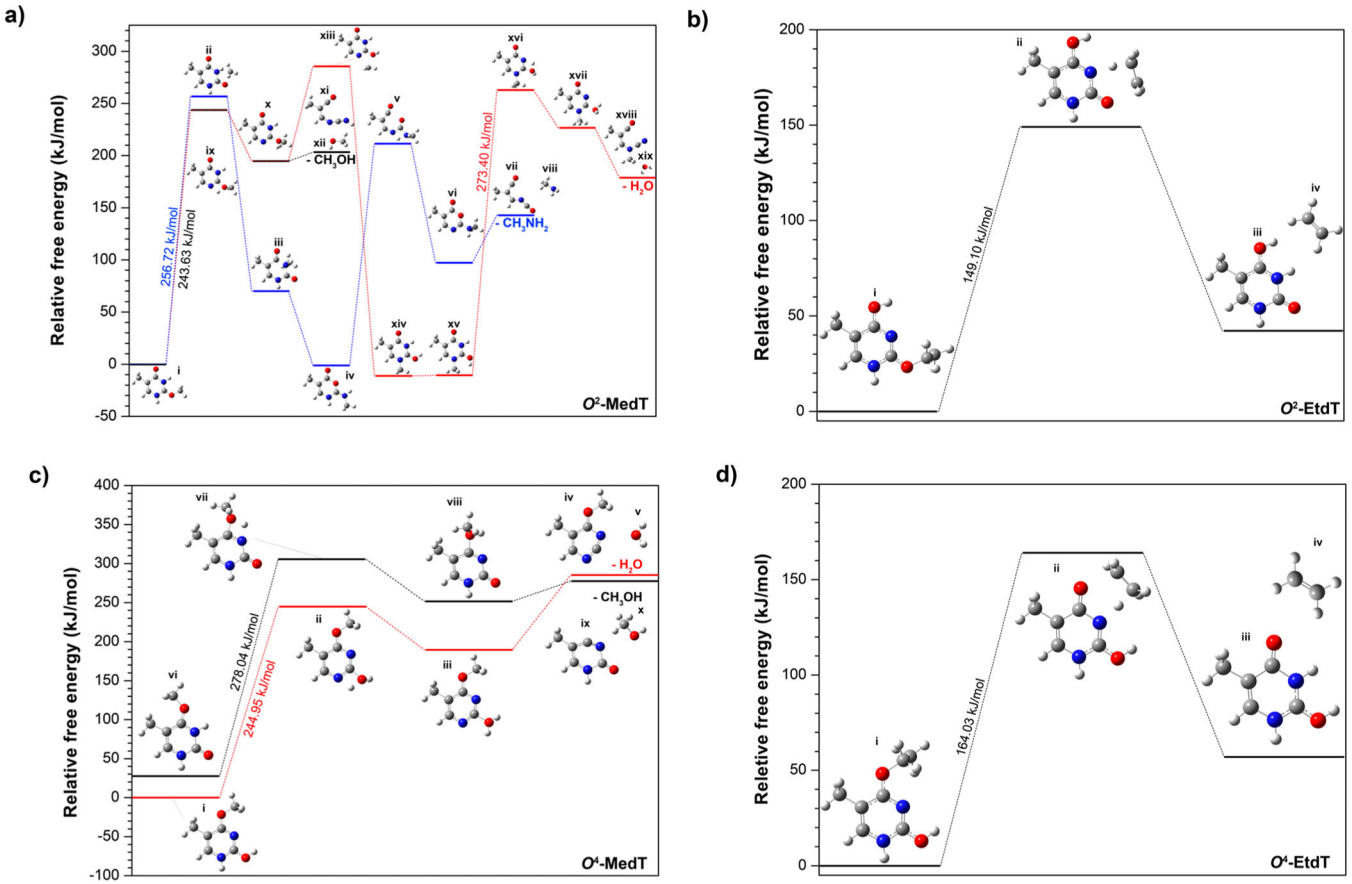

Figure 2.

DFT-calculated fragmentation pathways and energy barriers for (a) O^2-MedT, (b) O^2-EtdT, (c) O^4-MedT, and (d) O^4-EtdT at the B3LYP/6–311+G(2d,2p) level of theory.

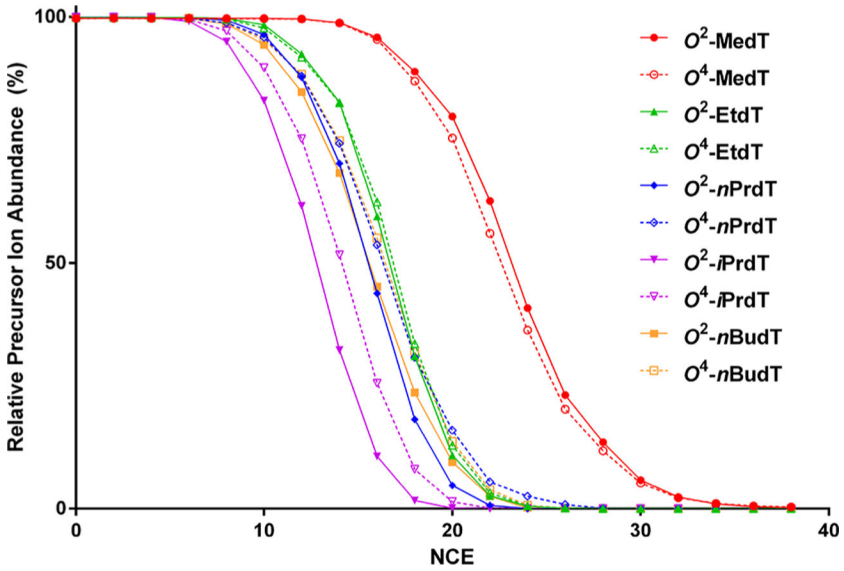

Figure 3.

Breakdown curves for the protonated ions of the nucleobase portions of O^2-alkyldT and O^4-alkyldT, as obtained from MS^3 with CID. NCE: normalized collisional energy.

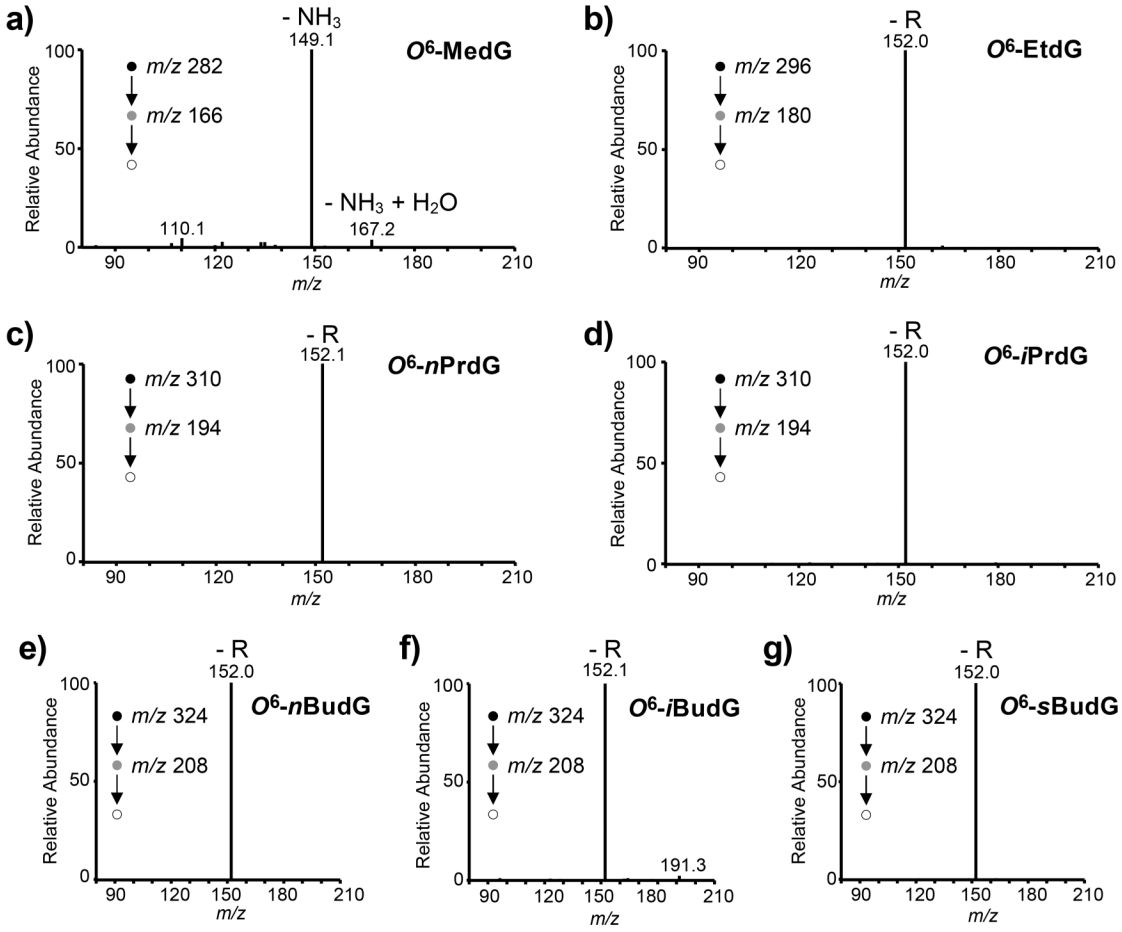

Figure 4.

MS^3 of (a) O^6-MedG, (b) O^6-EtdG, (c) O^6-*n*PrdG, (d) O^6-*i*PrdG, (e) O^6-*n*BudG, (f) O^6-*i*BudG, and (g) O^6-*s*BudG acquired from nLC-nESI-MS/MS/MS experiments.

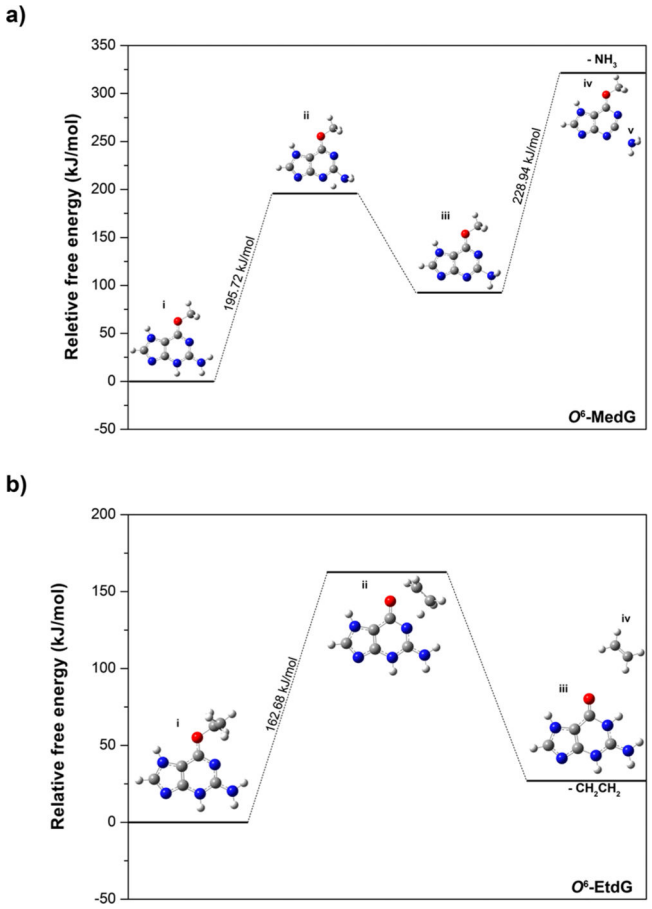

Figure 5.

DFT-calculated fragmentation pathways and energy barriers for (a) the elimination of ammonia from O^6-MedG and (b) the elimination of ethylene from O^6-EtdG via a six-membered ring transition state at the B3LYP/6–311+G(2d,2p) level of theory.

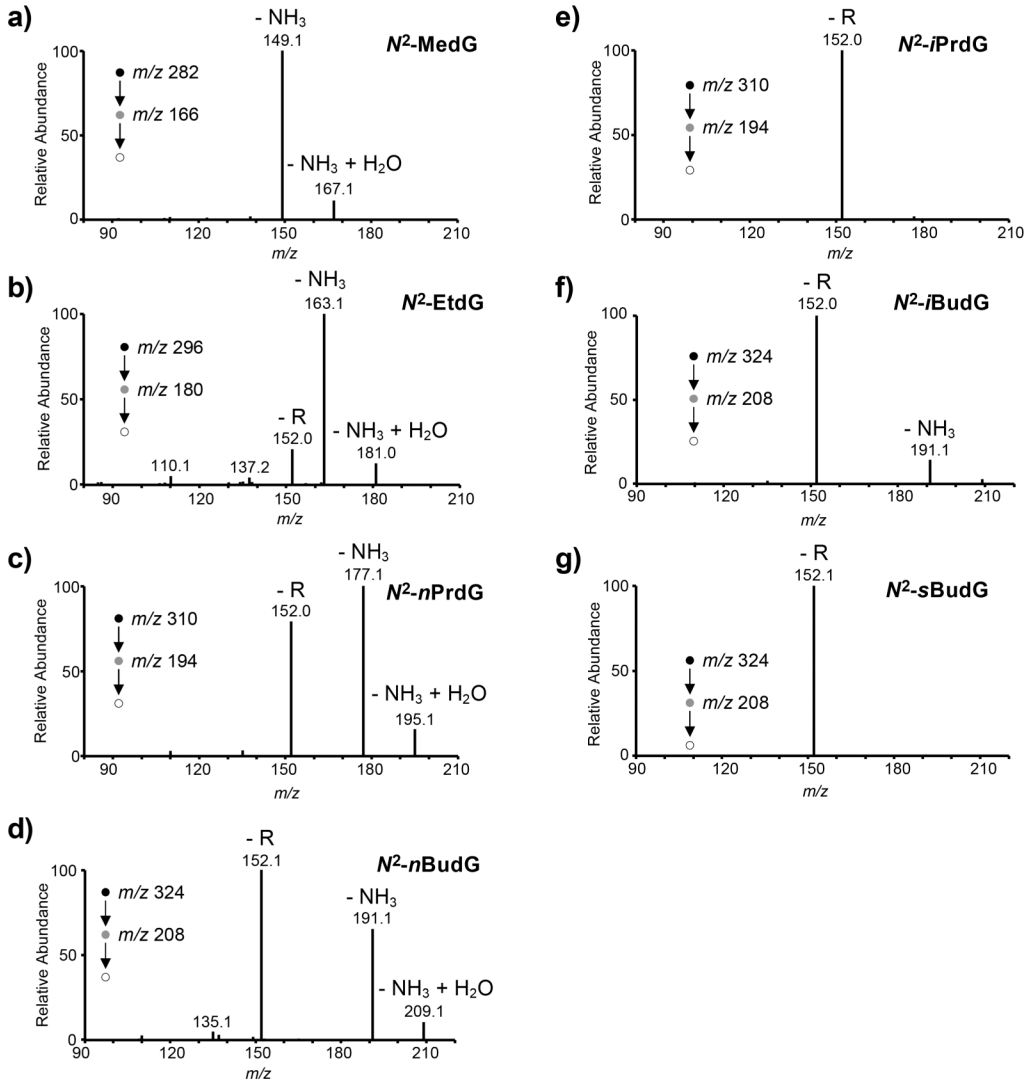

Figure 6.

MS^3 of: (a) N^2-MedG, (b) N^2-EtdG, (c) N^2-*n*PrdG, (d) N^2-*i*PrdG, (e) N^2-*n*BudG, (f) N^2-*i*BudG, and (g) N^2-*s*BudG obtained from nLC-nESI-MS/MS/MS experiments.

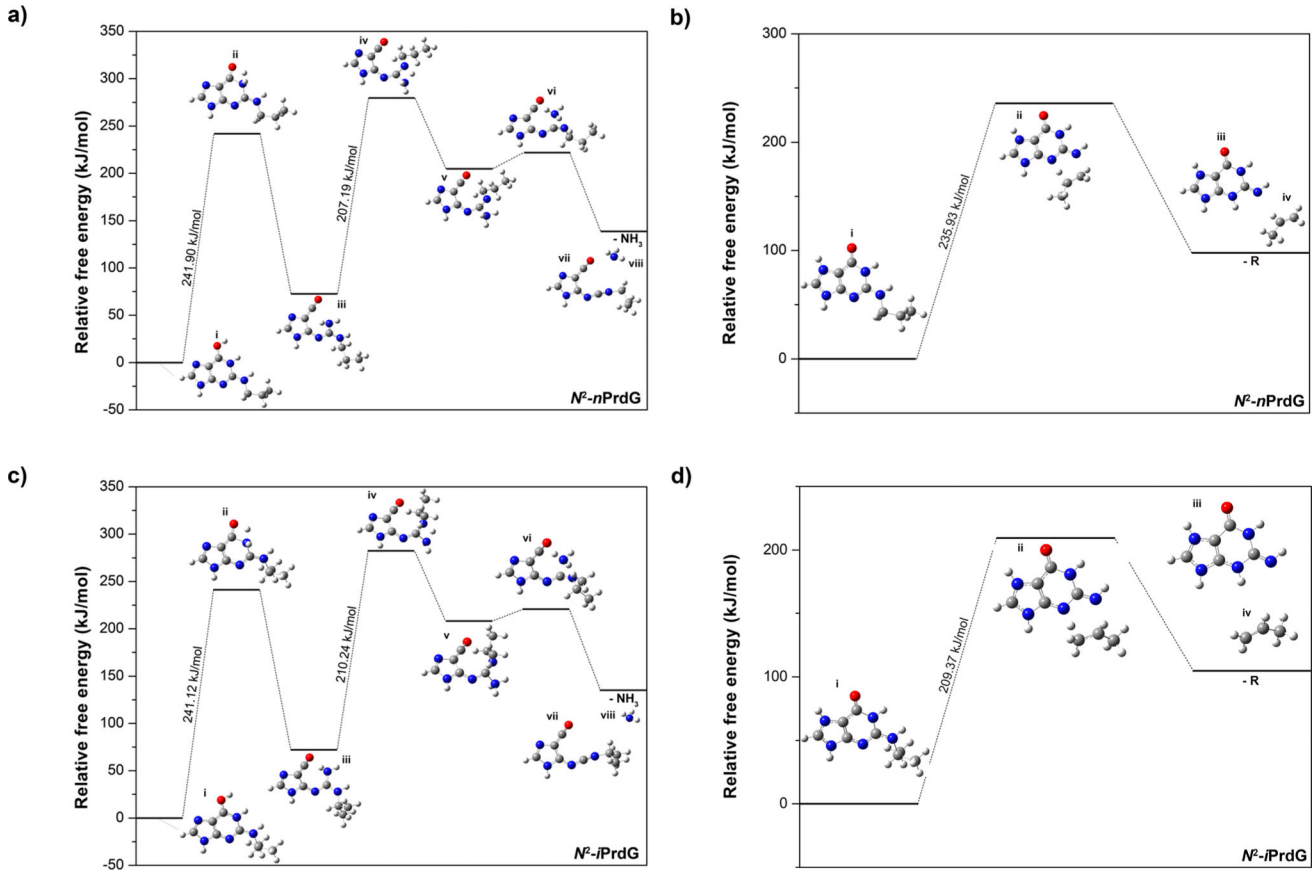

Figure 7.

DFT-calculated fragmentation pathways and energy barriers for the elimination of (a) ammonia and (b) alkene from N^2-*n*PrdG, and the loss of (c) ammonia and (d) alkene from N^2-*i*PrdG at the B3LYP/6–311+G(2d,2p) level of theory.

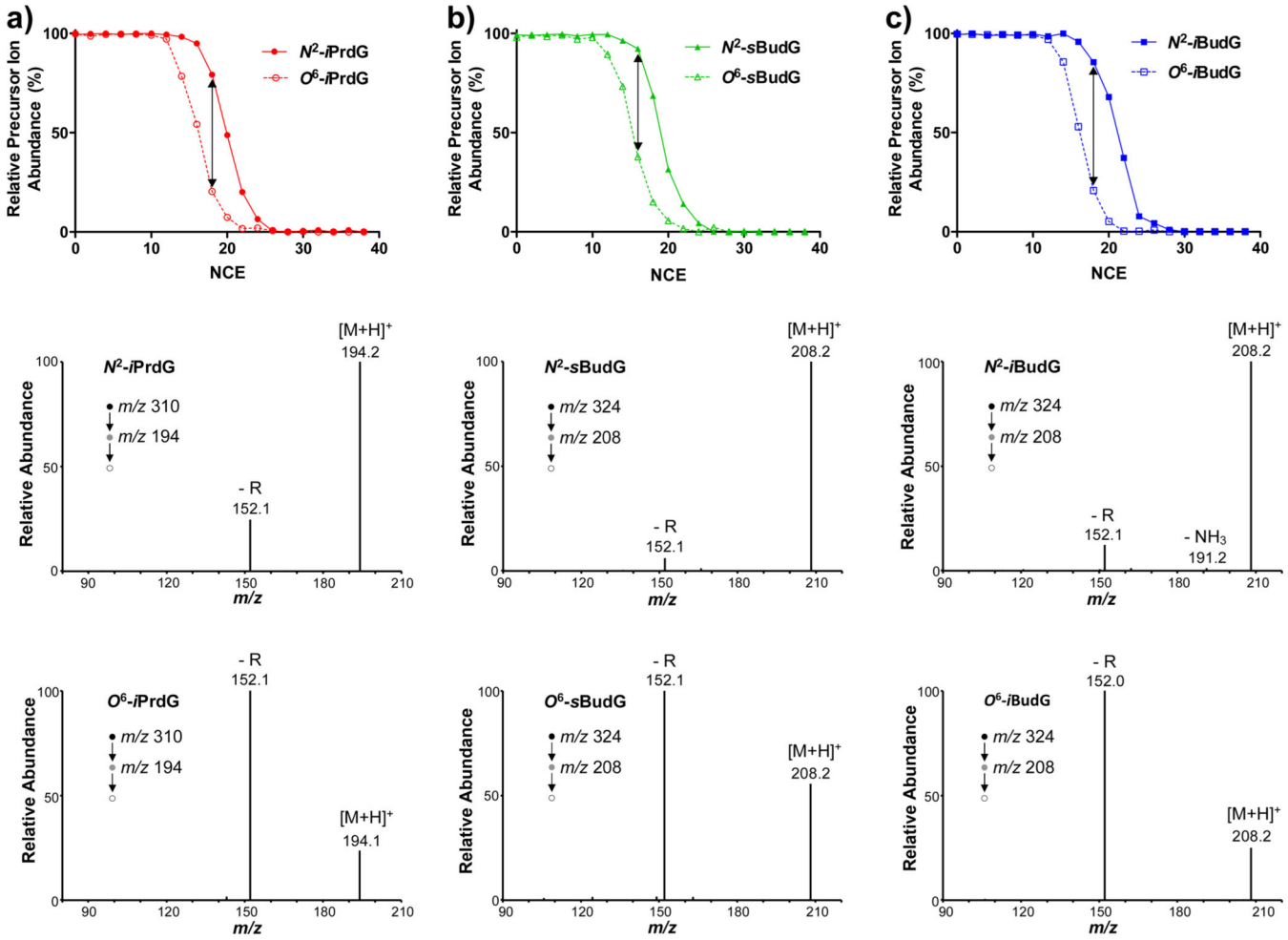

Figure 8.

Breakdown curves of protonated ions of the nucleobase portions of those O^6-alkyldG and N^2-alkyldG lesions with a branched chain alkyl group and the respective MS^3 spectra at the collisional energy yielding the largest difference in cleavage efficiency for the two regioisomers (indicated with double-headed arrows). The alkyl groups are (a) -*i*Pr, (b) -*s*Bu, and (c) -*i*Bu, respectively. NCE: normalized collisional energy.

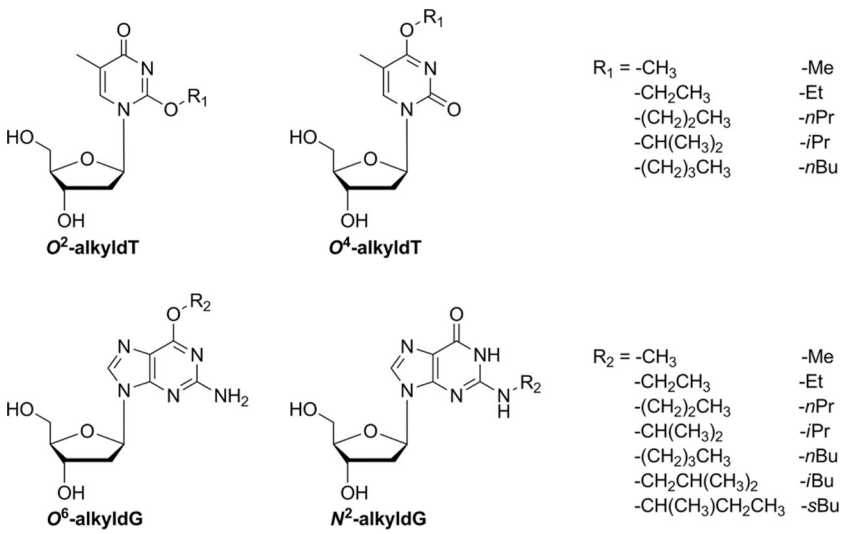

Scheme 1.
Alkylated Nucleosides Employed in This Study

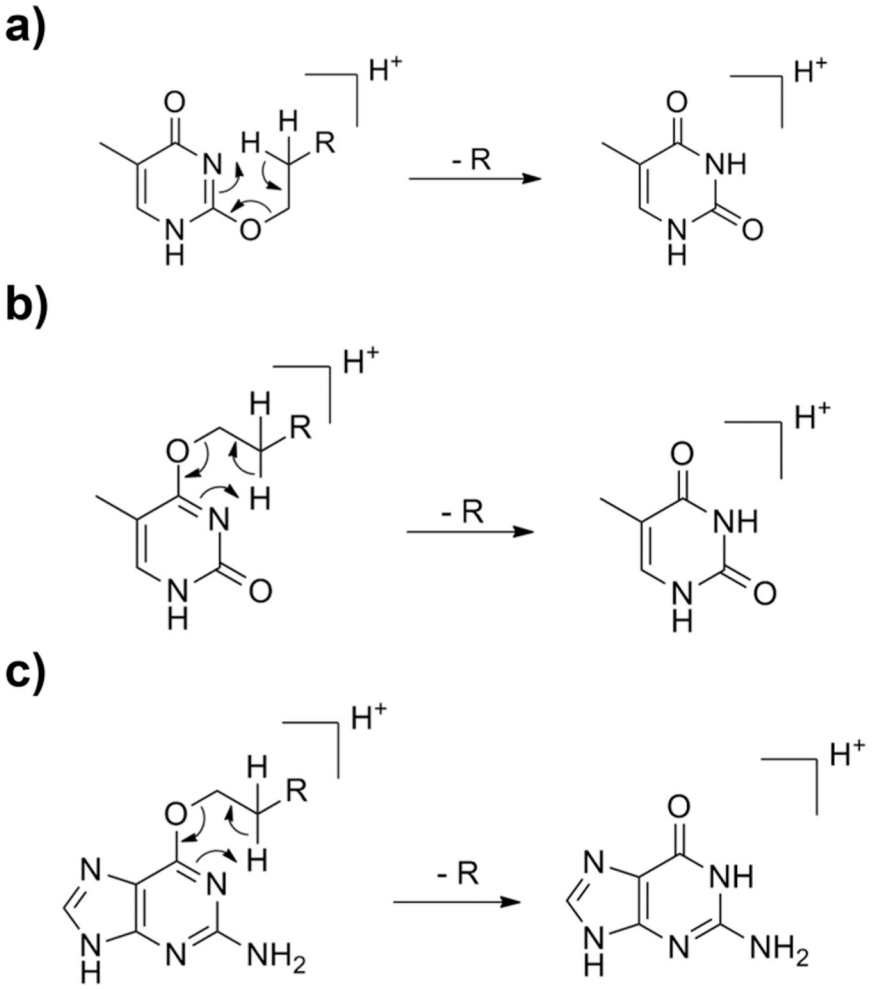

Scheme 2.

Proposed six-membered ring transition states for the elimination of alkene from (a) O^2-alkyldT, (b) O^4-alkyldT, and (c) O^6-alkyldG